

# Extracting BIM information for lattice toolpath planning in digital concrete printing with developed dynamo script: a case study

Yiwei Weng, Ph.D.<sup>1</sup>, Nisar Ahamed Noor Mohamed<sup>2</sup>, Brian Jia Shen Lee<sup>3</sup>, Nicole Jia Hui Gan<sup>4</sup>, Mingyang Li, Ph.D.<sup>5</sup>, Ming Jen Tan, Ph.D.<sup>6</sup>, Heng Li, Ph.D.<sup>7</sup>, Shunzhi Qian, Ph.D.<sup>8</sup>

**Abstract:** In this paper, a novel method for printing path design in the 3D Concrete Printing process (3DCP) has been developed and applied to a large-scale construction process. Despite that number of research works in digital concrete printing over the last decade, few studies have been applied to explore the way of automatically printing path design, specifically designing the printing path by directly extracting BIM information from the BIM platform in 3DCP. To obtain the BIM information and automatically design the printing path, a script package was developed using a single scripting environment called Dynamo - a plug-in of Revit. The proposed method was evaluated by the results of simulation and real-time printing. Compared with the conventional method, the simulation results show that the proposed approach can reduce the data loss from the 3D BIM model to the printing path generation. The real-time printing test implies that the proposed approach can be perfectly used to integrate BIM with 3DCP.

**Keywords:** Digital fabrication; 3D Concrete Printing; Building Information Modeling; printing path design

<sup>1</sup>Research Fellow, Singapore Centre for 3D Printing, Nanyang Technological University, Singapore. Email: ywweng@ntu.edu.sg

<sup>2</sup>Formerly, Research Associate, Singapore Centre for 3D Printing, Nanyang Technological Univ., Singapore.

<sup>3</sup>Formerly, Undergraduate Student, Singapore Centre for 3D Printing, Nanyang Technological Univ., Singapore.

<sup>4</sup>Formerly, Undergraduate Student, Singapore Centre for 3D Printing, Nanyang Technological Univ., Singapore.

<sup>5</sup>Research Fellow, Singapore Centre for 3D Printing, Nanyang Technological Univ., Singapore (Corresponding author). Email: limingyang@ntu.edu.sg

<sup>6</sup>Professor, Singapore Centre for 3D Printing, Nanyang Technological Univ., Singapore. Email: mmjtan@ntu.edu.sg

<sup>7</sup>Professor, Depart. of Building and Real Estate, The Hong Kong Polytechnic Univ., Hong Kong, China. Email: heng.li@polyu.edu.hk

<sup>8</sup>Assistant Professor, School of Civil and Environmental Engineering, Nanyang Technological Univ., Singapore. Email: szqian@ntu.edu.sg

## Introduction

Building Information Modeling (BIM) is a comprehensive construction management approach that covers the complete lifecycle of a building project (Chang and Shih 2013; Wang, Wei, and Xu 2018), including modeling, construction planning, cost estimation, and post-construction facility management (Elmualim and Gilder 2014). The unique characteristic of the BIM model is that it not only contains geometrical information but also embraces material, resources, equipment, and manufacturing data. Such a model with all the required data in a single package would be the ultimate digitization solution for the building and construction industry. Similar to BIM being a type of digital management and information sharing platform, digital fabrication, especially 3D concrete printing (3DCP), is considered as a digital manufacturing process in the construction sector, which makes it a perfect match with BIM technology to bring building and construction industry into the digital era (Wu, Wang, and Wang 2016a).

3DCP has many advantages over traditional manufacturing processes, especially for low-volume products with complicated geometries (Jiang et al. 2019; Lu et al. 2019). Conventional building and construction-related industries have been recognized as a significant resource consumer, high environmental stress, and relatively low productivity, as stated in many works. For example, Herczeg et al. (2014) reported that buildings account for 42% of the total energy consumption, 50% of the raw materials used, and 25% of the water consumed globally. Furthermore, poor performance in productivity also poses challenges in this area. The comparison of labor productivity in 20 countries implied that the US had the worst performance with an annual compound rate of -0.84% (Nasir et al. 2014). Similar to the US, the vast resources consumption and low productivity issues have also been found in other developed countries and regions, including the UK (Wahab et al. 2008), Singapore (Lim and Alum 1995), and Hong Kong (Lo, Fung, and Tung 2006). 3D printing is a potential approach to address the abovementioned challenges. This technology has experienced exponential growth in the past few years since both academia and industry have shown great interest in exploring this area (Bos et al. 2016; Gosselin et al. 2016; Khoshnevis 2004; Le et al. 2012). Its potential benefits of providing a safer production environment, reducing labor cost and material wastage, and increasing productivity have given this technology a huge boost for industry adoption (Rashid et al. 2020). Weng et al. (2020) revealed that a prefabricated bathroom unit fabricated by 3DCP achieves a reduction of 25.4% in overall cost, 85.9% in CO<sub>2</sub> emission, and 87.1% in energy consumption compared to the precast one. 3DCP also realizes a PBU with reduced self-weight (i.e., 26.2% lighter) and higher productivity (i.e., 48.1% improved) compared to the precast one. The above

enhancements were found to be ascribed to the formwork-free fabrication in 3DCP. More elaboration on the benefits of 3DCP can be found in (De Schutter et al. 2018).

3D concrete printing (3DCP), in which cementitious materials are extruded through a nozzle to construct a physical object in a layer-atop-layer manner based on a 3D model, is one of the 3D printing techniques being applied in the construction industry (Weng et al. 2019). In the construction industry, many attempts have been made to increase customization, reduce construction time, and improve productivity through 3D printing. Major contractors and academic institutes, like Foster and Partners (Wu, Wang, and Wang 2016b), Nanyang Technological University (Lim, Weng, and Pham 2020; Weng et al. 2019), Eindhoven University of Technology (Salet et al. 2018), and Swinburne University of Technology (Xia, Nematollahi, and Sanjayan 2019), have developed different types of 3D architectural modeling equipment and processes for printing 3D building models. Despite growing attention in recent years, 3D printing in architecture and construction is still in the early stage of development.

Many researchers have proposed the integration of BIM and 3DCP to facilitate digital construction. Arayici et al. (2011) showed that BIM could be used to create a small scale rapid prototyping model of a construction project. Ding et al. (2014) explored a BIM-based construction system, whereby BIM model data was fed into a manual slicing and code generation process. Wu et al. (2016a) discussed the potential of coupling 3D printing and BIM from exporting standard 3D printing file format to deeper system integration. Schutter et al. (2018) also mentioned that BIM could be the central software to manage the building process in the future. However, few of these studies have achieved a full automation process from BIM to 3DCP.

Furthermore, BIM is only a modeling software for 3DCP up to date, and other software is needed for processing the created 3D models to obtain the printing path. Consequently, the issues (such as data loss and data interoperability) may happen due to the data transfer between different platforms. Since BIM is a widely adopted platform in the construction sector for construction design, management, and information sharing, there is a need for 3DCP technology to be better integrated into the BIM platform, simplifying the workflow interacting with BIM software, and reducing the loss of data obtained from BIM model.

This work is motivated by the research gap above, and a novel process from BIM to physical parts printed by 3DCP is proposed. In the proposed approach, a BIM software integrated with a script package is used to filter and slice a digital model, produce a printing path, generate infills, create machine code, which was sent to a 3D concrete printer. Afterward, the physical object can be printed by the 3D concrete printer. In order to demonstrate the feasibility and effectiveness of this approach, the proposed script package was developed using Dynamo and integrated into BIM software Autodesk Revit. A small-scale digital model was then designed in Autodesk Revit and printed by a 3D concrete printer.

### **3D Concrete Printing And Bim Integration**

3DCP is a revolutionary technology in the construction sector. It provides the opportunity to make the construction process a fully digitalized one through shifting from a well-developed CAD model to automated construction (Lu et al. 2019). Productivity can also be increased due to the integration of digital design and construction activities by shortening construction time, improving quality, and reducing costs (Wu et al. 2016a). This vision was shared by Agarwal et al. (2016), and they suggested a transformation to the digital construction process through the combination of existing technologies including rapid digital mapping, BIM, digital collaboration, internet of things, design, and 3DCP. As a consequence, potential errors can be minimized, and construction management can be improved through digitalized processes from design to production.

However, according to Wu et al. (2016a), similar to other additive manufacturing (AM) technologies, 3D concrete printing process from a design to an actual printed object is long and complicated, consisting of six steps: digital modeling, exporting, slicing, connecting, printing and post-processing. The 3D designed model can be created through a traditional approach in CAD software and then converted to Standard Tessellation Language (STL) format file, which is commonly used in AM technologies. Slicing software is used to slice the STL file, then the tool path and machine code are generated accordingly before being fed into a 3D printer. This existing process is not robust because it is vulnerable to data loss and is ineffective due to constant data transfer from one software to another (Tibaut, Rebolj, and Perc 2016).

In order to simplify this tedious and time-consuming process, a revised design process flow is proposed. BIM is designed to have the ability to extend its functions (Eastman et al. 2011), a plug-in can be developed to implement functions of slicing, and send the generated machine code directly to a 3D concrete printer, as schematically shown in Fig. 1. Compared with the traditional 3DCP process (Fig. 1), in this proposed approach, various steps, including 3D modeling, slicing, path generation, and machine code generation, are all undertaken in the same BIM platform. With embedded default inputs and a standby 3D concrete printer, it is possible to consolidate all the steps into a fully automatic operation, which could significantly facilitate the workflow from digital design to final printed objects.

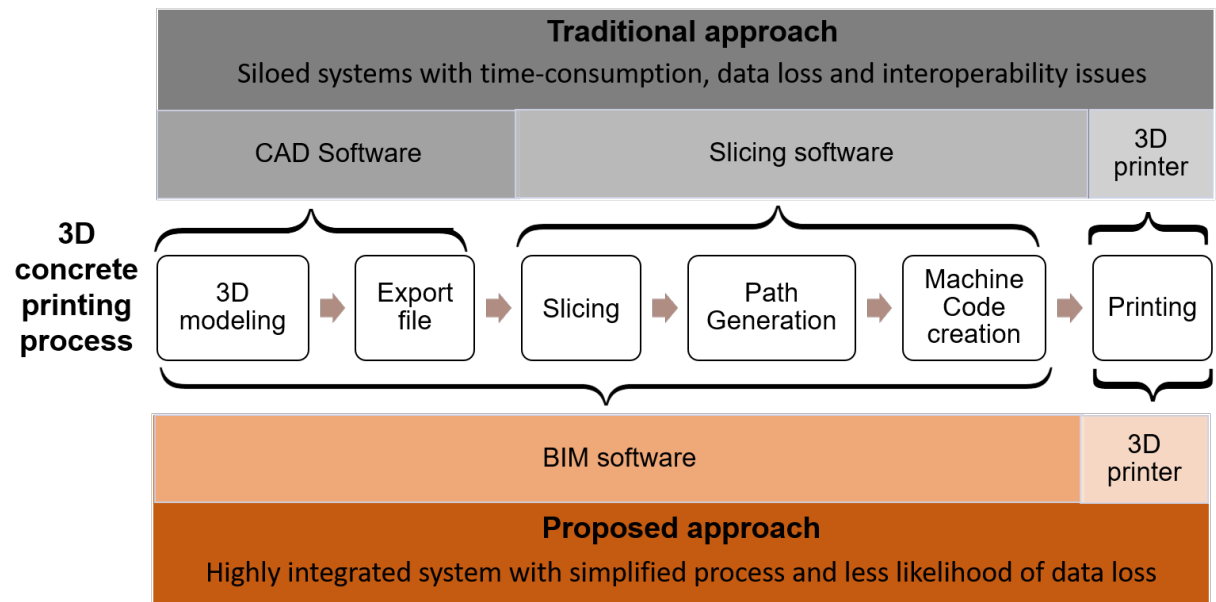


Fig. 1.Steps and platforms of 3D printing in traditional and proposed approaches

## Methodological Development

To demonstrate the proposed process, a script package was developed using Dynamo and integrated into BIM software Autodesk Revit. Dynamo is an open-source component technology for visual programming. It uses visual scripts in the form of nodes and links, where each or a group of nodes performs a defined function. The workflow of this self-developed script package is shown in Fig. 2, and the final target of this work is to adopt the presented approach and print a predefined concrete wall as a practical demonstration.

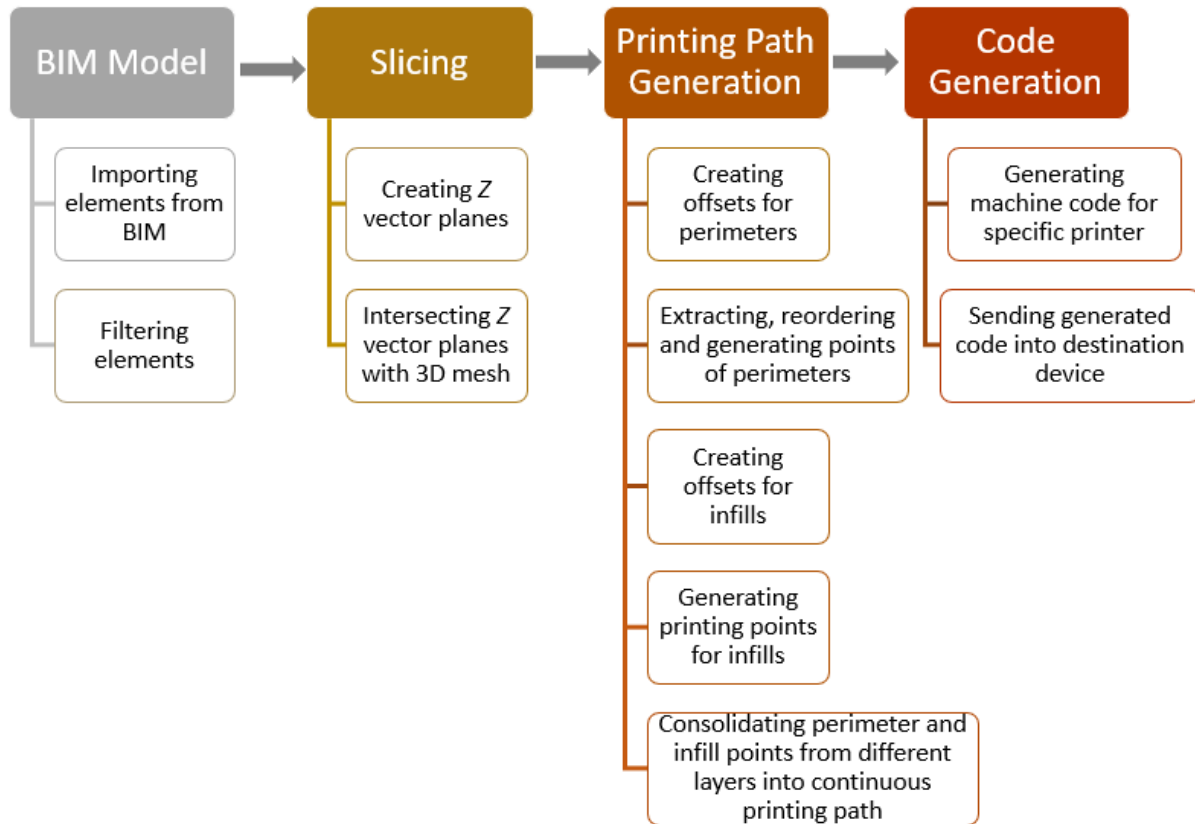


Fig. 2. Flow chart of the script package developed to execute the process from BIM to 3D concrete print

### BIM Model Importing, Filing, and Data Collection

A BIM model can be created with elements made of various materials (e.g., brick, wood, glass, and concrete) and categorized as different structural components (e.g., doors, windows, floors, ceilings, and walls). These data can then be used as the indicators to filter out components required for the 3DCP. Fig. 3 shows the BIM model used in this work, where a Revit model has a series of wall segments and a concrete floor. The wall is made of two types of materials: brick in red and concrete in gray. The workflow of this part is schematically shown in Fig. 4. In detail, the "concrete" and "wall" are two keywords for printing element selection, and only the wall segment made of the concrete material could be filtered out through the customized "Filter Concrete Elements" function in the script package, as illustrated in Fig S.1 (supplementary materials).

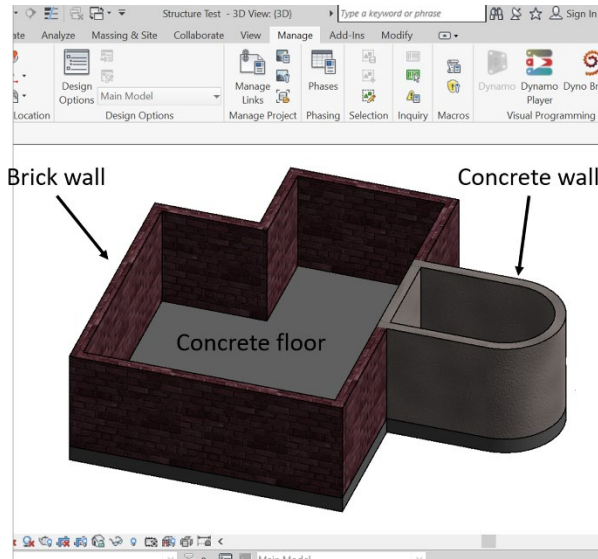


Fig. 3 Sample Revit model composed of a concrete wall, a brick wall as well as concrete floor

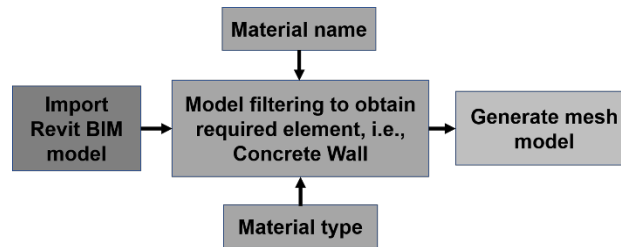


Fig. 4. The workflow of obtaining mesh BIM model

Afterward, the 3D model obtained from the BIM model is converted into a Dynamo mesh, which is a collection of quadrilaterals and triangles that represents a surface or solid geometry. By using both quadrilateral and triangular tessellation schemes, greater flexibility can be achieved in 3D modeling than in STL format, especially for curved surfaces and edges. The filtered concrete wall from Fig. 3 is then converted into a meshed object through the "Mesh Element" function in the script package,

### 3D Model Slicing

After obtaining the mesh element, in this step, the created Dynamo mesh is cut into horizontal planes, of which the profile is computed for further path generation. The workflow of this part is plotted in Fig. 6. Firstly, the meshed object is used to locate the upper bound and the lower bound of the structure and its respective Z-coordinate. A series of Z vector planes (horizontal planes) are generated from the layer height, which can either be the default value or

user input value, as illustrated in Fig. 5 (a). Each plane is then used to intersect the mesh object and produces the surface contour in the form of multiple layers of the polygon. The visual programming uses *Plane.ByOriginNormal* and *Mesh.Intersect* as critical nodes to generate vector planes and surface contours, respectively. Taking sample Revit mesh model in Fig. 3 as an example, the final sliced model through the developed function is shown in Fig. 5 (b). The detailed visual programming for this part is shown in Fig S.2.

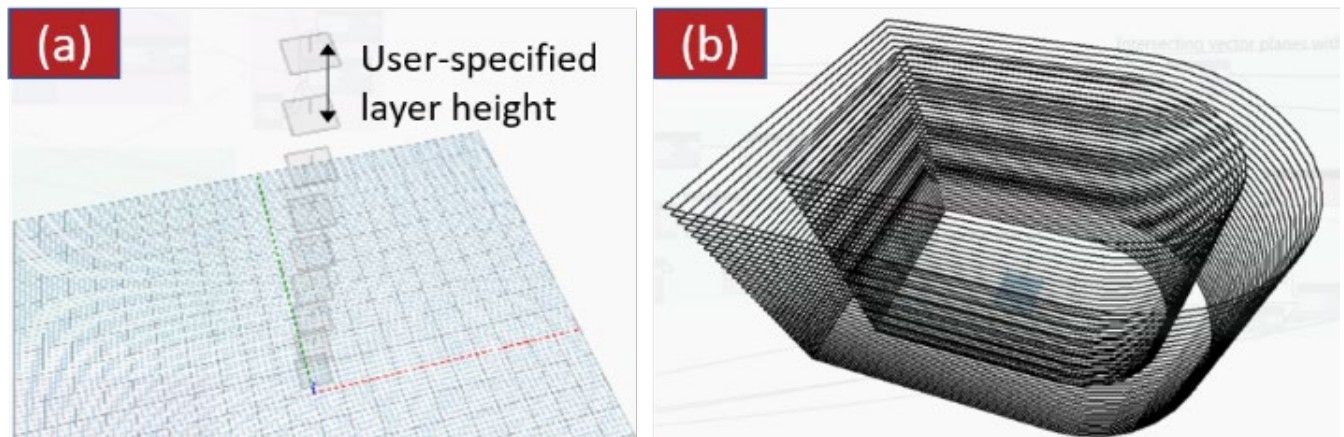


Fig. 5 Slicing process: (a) Generated Z planes with user-specified layer height; (b) An example of the final sliced model

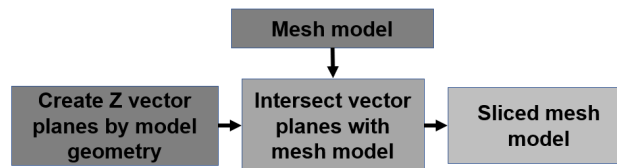


Fig. 6. Workflow for creating sliced BIM model

## Printing Path Generation

### (1) Creating offset for perimeter and infill walls

After the slicing step, the printing path can be created from the profiles of each layer. In this case study (concrete wall element in Fig. 3), there are two types of the path that define the printing contours of walls: the perimeter printing path and the infill printing path. The perimeter printing path defines the movement of a printer nozzle to print the external surface of the wall. It must be offset by half an extrusion width away from the surface boundary to avoid exceeding the perimeter dimensions of the object. Similarly, the infill printing path is defined within the surface contours of the walls and offset by a full extrusion width away from the perimeter printing path. As there are numerous options of



infills available for other AM methods (Vicente et al. 2016), a Zig-Zag lattice infill pattern was selected in this self-developed script package for the demonstration purpose. The continuous Zig-Zag lattice infill pattern are selected mainly due to two reasons: (a) a continuous printing path design is chosen to bypass the challenge of the accurate start and stop flow control in the current delivery system, where the air trapped in material leads to a long time dynamic response (Li et al. 2013); additionally, continuous printing path can reduce the delay time and overall operation time (Diggs-McGee et al. 2019); (b) the Zig-Zag lattice infill pattern is chosen to provide additional support to the whole printed structure and thus enhance the structural stability, and the spaces in between the infill pattern can be used to place structural steel reinforcement or run mechanical and electrical services within the walls. More discussions on the impact of printing path on the printed structure properties can be found in (Buswell et al. 2018).

## **(2) Extracting, reordering, and generating points of perimeters and infill**

Two offset curve paths were created based on the external surfaces, and control points were generated along the offset lines of the inner and outer boundaries. It should be noted that the term "curve" is a generalization for different sorts of curved shapes, including straight lines. Compared with straight lines modeled simply as a single curve with a start and end point, curvatures are more complex and modeled using multiple smaller curves, as shown in Fig. 7. The list of curves for each layer is arranged randomly, which indicates that the curves in the second layer are not necessarily in the same sequence as those in the first layer. A reordering operation, which aligns the list of curves in each layer with the order in the previous layer, assists with a better arrangement of the curve sequence for each layer to allow for convenient manipulation of the points to generate the tool path. The workflow of this part is shown in Fig. 8, and the visual programming for the perimeter wall is shown in Fig S.3.

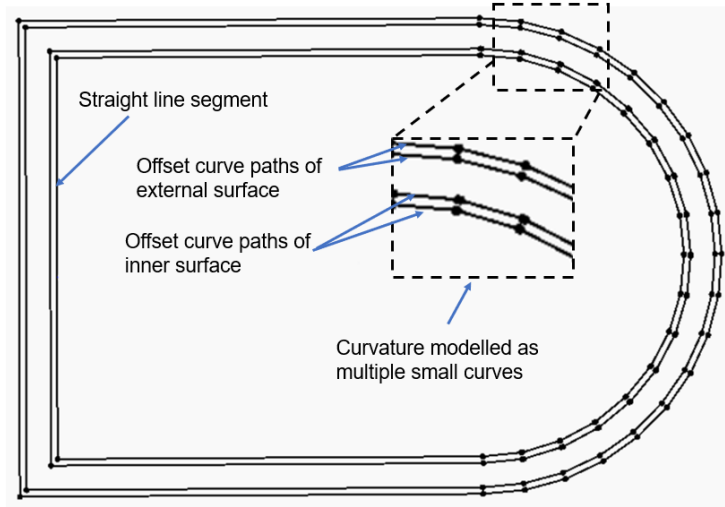


Fig. 7 Straight lines and curvatures are decomposed into constituent curves

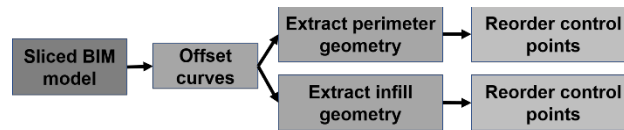


Fig. 8. The workflow of extracting and reordering the perimeter and infill walls

### (3) Creating infill path

The workflow of this part is shown in Fig. 9. Firstly, the control points in the inner fill geometry and outer infill geometry are obtained and reordered. After the points in inner and outer infill boundaries are appropriately ordered, lines are drawn to join these control points using suitable functional nodes in an alternating manner to create the sinusoidal wave Zig Zag pattern. Since the sharp corners in the infill are undesirable to print, a sinusoidal wave was used to smoothen the infills. The central nodes to create offsets and curve infills are *DynamoClipper.OffsetPolys*, self-developed ordering function, and Non-Uniform Rational Basis Spline (NURBS) package. The visual programming in Dynamo is shown in Fig S.4. Several examples are taken to show the result of the visualization of offset boundaries, control points, and smooth infills, as illustrated in Fig. 10.

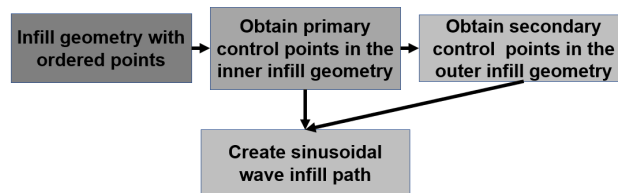
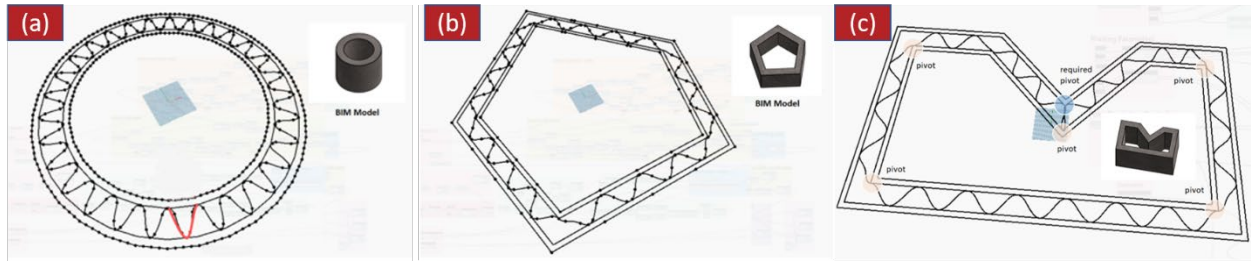


Fig. 9. Workflow of creating infill curve

211



212

213 Fig. 10. Visualization of offset boundaries, control points, and smooth infills of example geometries: (a) Simple  
214 circular structure; (b) Simple convex structure; (c) Simple concave structure

215

#### 216 (4) Consolidating perimeter and infill points from different layers into continuous printing path

217 Before generating the machine code for printing, the printing path of each layer should be consolidated and arranged  
218 to constitute a continuous printing path, i.e., the transition between each consecutive layer should be considered. Since  
219 the 3D concrete printer used in this study prefers a continuous printing path without additional start and stop, the start  
220 point of the next layer should be as close as possible to the end point of the previous layer. The distances between  
221 each point of the next layer and the end point of the previous layer are computed. Another reordering operation is  
222 conducted to arrange the next layer starting from the point with the shortest distance to the end point of the previous  
223 layer. Then, a single list of consecutive points is consolidated from all the layers. The workflow of this part and visual  
224 programming in Dynamo are shown in Fig. 11 and Fig S.5, respectively. The visualization of the completed printing  
225 path of an example geometry is shown in Fig. 12, and the connection line between layers can be found in Fig. 12 (b).

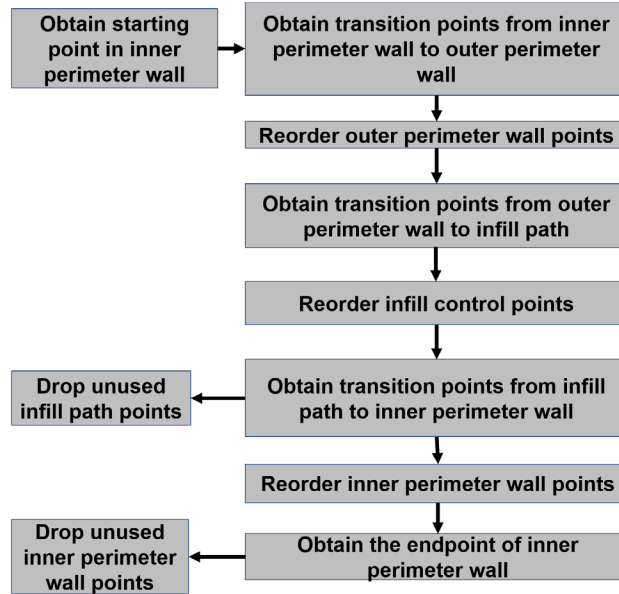


Fig. 11. The workflow of generating continuous printing path

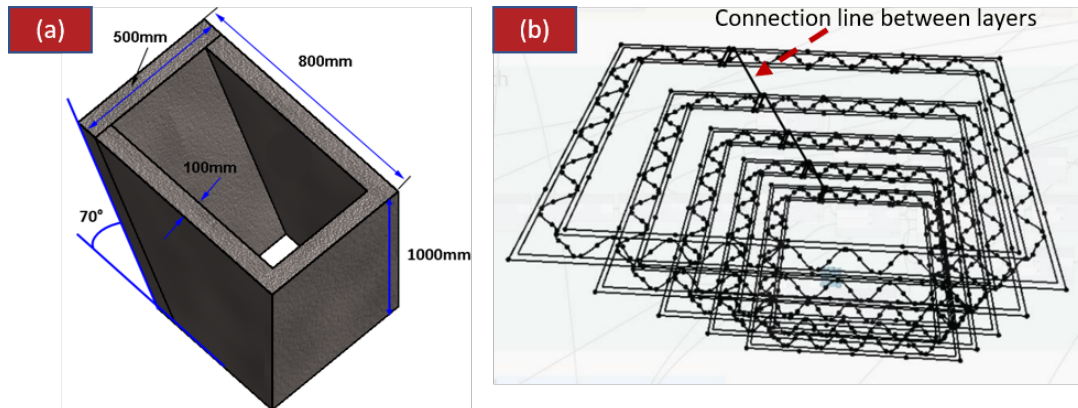


Fig. 12. The geometry and the visualization of the completed continuous printing path of a slanted wall: (a) The physical BIM model; (b) Generated continuous printing path of different layers, where different layers are connected.

### Machine Code Creation

After consolidation, the final step in the proposed process is to convert the information of these points into machine code. The x, y, and z coordinates of each point are extracted and converted to machine-specific code format. With other machine-specific beginning and ending code, the coordinates of machine code are written into a single file or sent directly to the 3D printer, depending on the operation interface of the specific 3D concrete printer. The workflow and visual programming for this function in Dynamo are shown in Fig. 13 and Fig S.6, respectively.

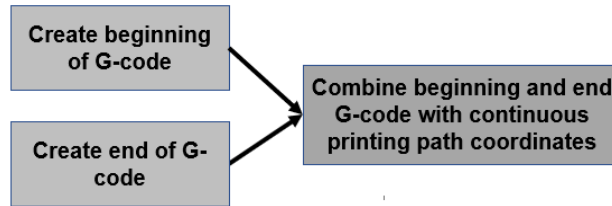


Fig. 13. Workflow of generating G-code

### Visualization: Integration of BIM Software and 3D Concrete Printer

A plug-in button is created in Revit workspace for a straightforward method to access the entire workflow, as shown in Fig. 14. With proper default setups, the processed information could be directly sent the digital design from Revit to a standby 3D concrete printer to construct the physical object. Before the script works, the inputs for the printing path generation are required to fill in, as indicated in Fig. 14. The inputs include printing speed, layer height of printed filaments, extrusion width, and density of infill, as shown in Fig. 14.

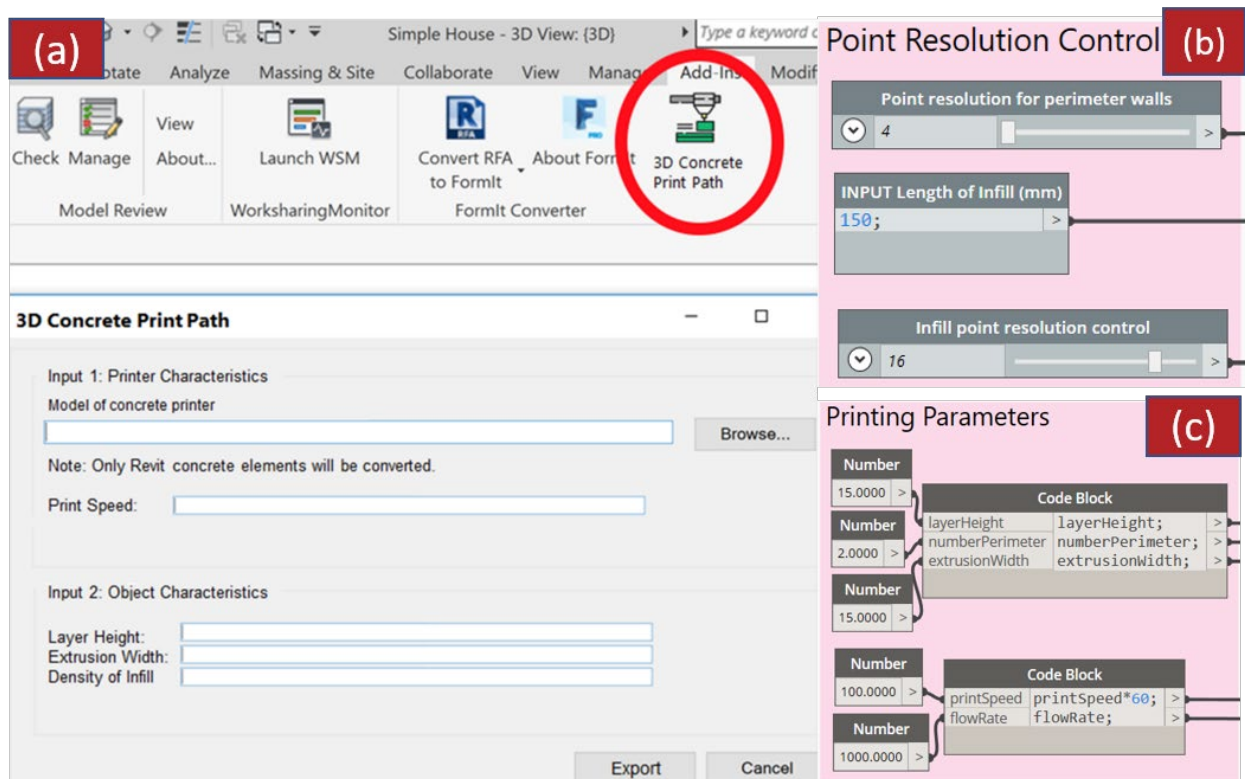


Fig. 14. The integrated plug-in button of sending digital design from Revit to a 3D concrete printer: (a) User interface; (b) Visual programming for point resolution control; (c) Visual programming for input printing parameters

## **Experimental Validation**

### **Materials and Mixture Proportion**

The material formulations used for printing consists of Ordinary Portland Cement (OPC, ASTM type I, Grade 42.5), Class F fly ash, superplasticizer (SP, ADVA 181N, GCP applied technologies), accelerator (MasterRoc SA160, BASF Pte. Ltd), silica fume (SF, undensified, Grade 940, Elkem company), silica sand and tap water. Two types of silica sands were used for printing, i.e., 0.26-0.6 mm ( $F_1$ ) and 0.15-0.25 mm ( $F_2$ ). The chemical compositions of fly ash and OPC could be found in (Weng et al. 2018). The particle size distribution of OPC, fly ash, and silica fume could also be found in (Weng et al. 2018).

The mixture formulations used for printing are shown in Table 1. A forced action mixer with an 80 L capacity (Soroto Pte. Ltd) was used for mixing materials. In the mixing phase, the raw powders were mixed for 5 min with 30 rpm. Then, the tap water was added and mixed for 5 min with 30 rpm, followed by 5 min with 40 rpm. After that, SP was added and mixed for 10 min with 40 rpm. Finally, the accelerator was introduced and mixed for 5 min with 50 rpm

### **Printing Setup**

A gantry printer was used for printing (Weng et al. 2018). This gantry printer uses a MITSUBISHI M70 Series CNC controller, which can take input from memory, CF card, USB port, and Ethernet. A circular nozzle of 15 mm in diameter was used for printing. A delivery system was used to pump cementitious materials to the nozzle through a hose with 3 m in length and 25.4 mm in inner diameter. The nozzle travel speed was 100 mm/s, the pumping flow rate was 0.9 L/min, and the layer height was 10 mm.

### **Case Study: Printing Path Generation for Printed Model**

A digital 3D model was designed in Revit, as shown in Fig. 3. The wall thickness and height of this model were 100 mm and 500 mm, respectively. The method, mentioned in Section "BIM Model Importing, Filing, and Data Collection", was used to obtain the mesh model of the filtered concrete wall in Dynamo. Then, the detailed steps to generate the printing path and machine code for printing are discussed as follows:

## Offset determination

After the slicing step, the printing path was generated from the profile of each layer. According to the method discussed in Section "Printing Path Generation", the offsets of the perimeter and infill printing paths of the concrete wall were defined through *DynamoClipper.OffsetPolys* node. The result is two sets of the polygon for every layer: one for the perimeter printing path, the other for the infill printing path, as illustrated in Fig. 15.

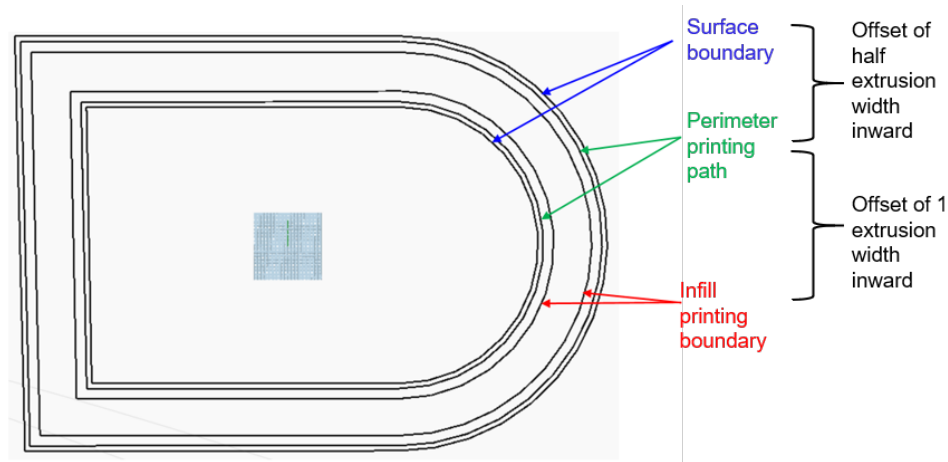


Fig. 15 Polygon offsets from surface boundary to perimeter and infill paths for a single layer

## Primary and secondary points generation for infills

As shown in Fig. 16, two sets of control points were defined to generate the infills: the primary points on the inner infill path and the secondary points on the outer infill path. To define the primary points, the lengths of each curve in the inner infill polygon of each layer were calculated. An infill parameter known as the infill length was defined or inputted by the user. The infill length was used to determine the number of divisions to divide each curve. The minimum number of divisions was rounded up to a value of 1, in instances where the curve length was smaller than the infill length. The curve divisions were expressed in terms of curve parameters and their respective points obtained through *Curve.PointAtParameter*.

The next set of control points to be established were the secondary control points. To obtain the sinusoidal infill pattern that travels between the outer and inner infill polygons, the secondary points were defined on the outer infill polygon and symmetrically staggered from the primary points. To achieve this, it was essential to calculate a secondary list of parameters along the inner infill polygon that are staggered from the primary parameters. The secondary points were

obtained from the secondary parameters through the *Curve.PointAtParameter* node and subsequently projected onto the outer infill polygon using the *Point.Project* node. The result is two sets of control points that are staggered from one another, as shown in Fig. 16.

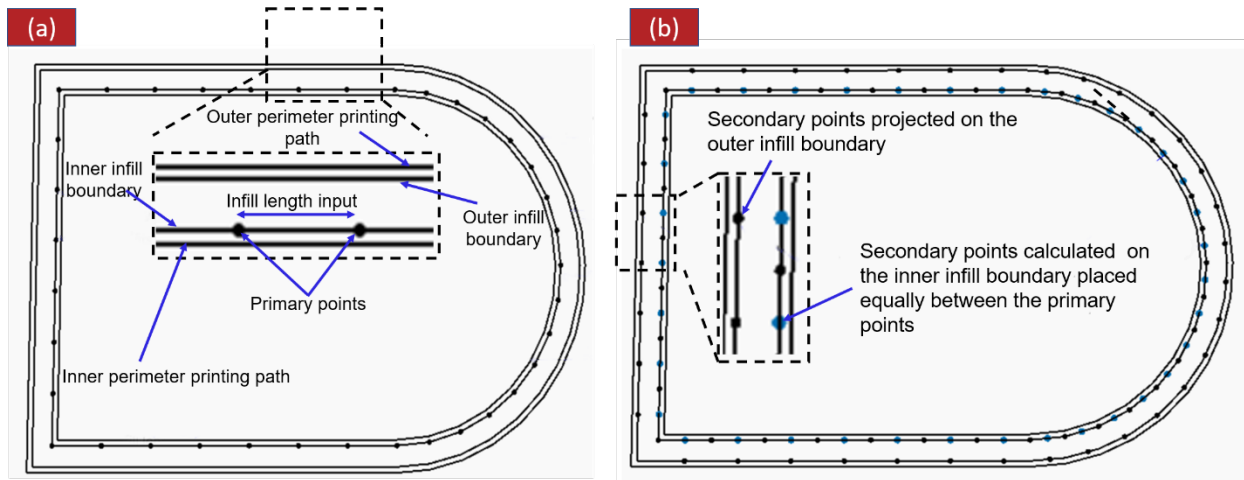


Fig. 16 Two sets of control points to generate the infills (a) primary points on the inner infill boundary; (b) secondary points on the outer infill boundary are generated from primary points

### Sinusoidal infills generation

Established control points imitated the general shape of the sinusoidal infill. Hence, the points, obtained from Section "Primary and secondary points generation for infills", formed a series of straight lines, which ran between the inner and outer infill polygons. These straight lines served as baselines for obtaining the third set of control points to define the final infill pattern of a sinusoidal curve. The node *NurbsCurve.ByPointsTangents* in Dynamo offers a convenient way of creating a sinusoidal curve. The node requires the inputs of the control points, start tangents, and end tangents to create a NURBS curve. Additionally, tangents to the inner infill polygon at the primary control points also need to be calculated through *Curve.TangentAtParameter*. The result is a smooth sinusoidal infill pattern, as shown in Fig. 17 (a) and (b).

The NURBS curve is expressed as points since the final G-code output is in the form of points. To preserve the smoothness of the curvature, the NURBS is approximated using *Curve.ApproximateWithArcAndLineSegments*. The resulting NURBS curve is expressed as multiple simple curvatures, consequently leading to a large number of points to express the sinusoidal curvature and an excessively large G-code size. Therefore, an infill point resolution control



is implemented to offer the user a choice to either increase the number of points to express the infill or decrease it. The infill point resolution control is a divisor, which reduces the total number of points to express the infill evenly by the defined amount. An infill point resolution value of 1 would mean no infill point reduction (Fig. 17 c), and a value of 2 would uniformly halve the number of points to express the sinusoidal infill. In this printing validation, a value of 16 was considered as a reasonable balance between maintaining the smoothness of the sinusoidal curvature and fewer number of points, as shown in Fig. 17 (d).

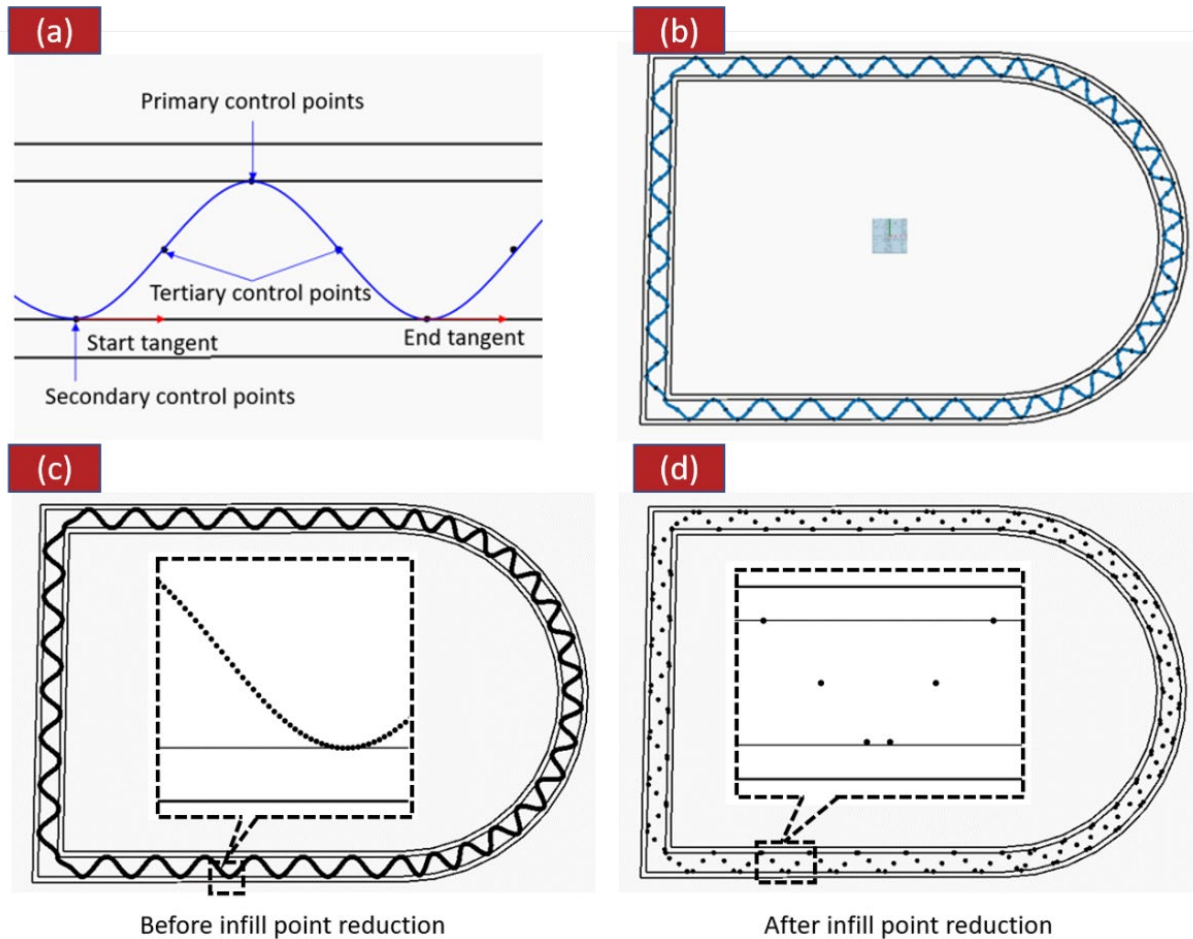


Fig. 17 Sinusoidal infill generation: (a) Sinusoidal infill pattern created by *NurbsCurve.ByPointsTangents*; (b) Sinusoidal infill pattern in the printing path; (c) No infill point reduction (infill point resolution value is 1, points are so dense that they appear to be a continuous curve) and (d) After infill point reduction (infill point resolution value is 16, only 1/16 points are shown compared to the (c))

331

332

333

334

335

336



338

340  
341  
342  
343  
344

- 345  
346  
347  
348

b. If two or more straight edges were of the longest length, the start point would be located at one-fourth of the length of the first straight-edge in the list, which is certainly depending on the printing direction and order of the list.

(2) If no straight edges were presented in the structure, the start point would be located at one-fourth of the first curve length.

The print path then proceeded along the innermost perimeter printing path in an anticlockwise direction up to three-fourths of the length of the first printing edge. At the three-fourths mark, the print path cut across and transition to print the outermost perimeter printing path in the anticlockwise direction. The first loop ended an extrusion width away from the transition line.

The second printing loop printed the infill but in the clockwise direction, as shown in Fig. 18. The second loop start point was obtained using the *Point.Project* node, where the end point of the first loop was projected onto the infill printing path geometry. The loop then follows the order of points of the infill printing path. The ending point of the second loop was the projected point of an extrusion width away from the first loop transition point. The second loop ended and transitioned across to the inner perimeter printing loop to print the final loop.

The third printing loop printed the remaining portion of the innermost perimeter printing path, following the same direction of the first loop, anticlockwise, as shown in Fig. 18. The endpoint of the third loop was set at an extrusion width away from the start point of the first loop, and also marked the end of the printing for the first layer. Subsequent layers were then printed in the same fashion, a similar sequence of points for the individual layer but with different layer height coordinates.

### **Machine code generation for printing**

The printing path, as elaborated in Section "Tool path generation", was then expressed in G-code format for the gantry printer described in Section "Printing Setup". The main body of the G-code was generated by going through the entire list of printing path points and converting the point coordinates to the corresponding G1 command as a string. The machine-specific control codes, such as setting origins, starting and stopping pumps, and move the nozzle back to

initial position, were attached to the beginning and the end of the printing path codes. The final generated machine code string was then outputted for printing.

### Printing Validation

The entire printing process was completed within 1.5 hours. Cementitious materials were mixed in batches and then fed into the pump before delivery to the gantry printer. Then, the gantry printer deposited the materials according to the machine code generated by the developed script package. The printing process, including the first layer of the printed structure, the top view of the product being printed, and the final printed product, are shown in Fig. 19, which demonstrates the printing path in practice.

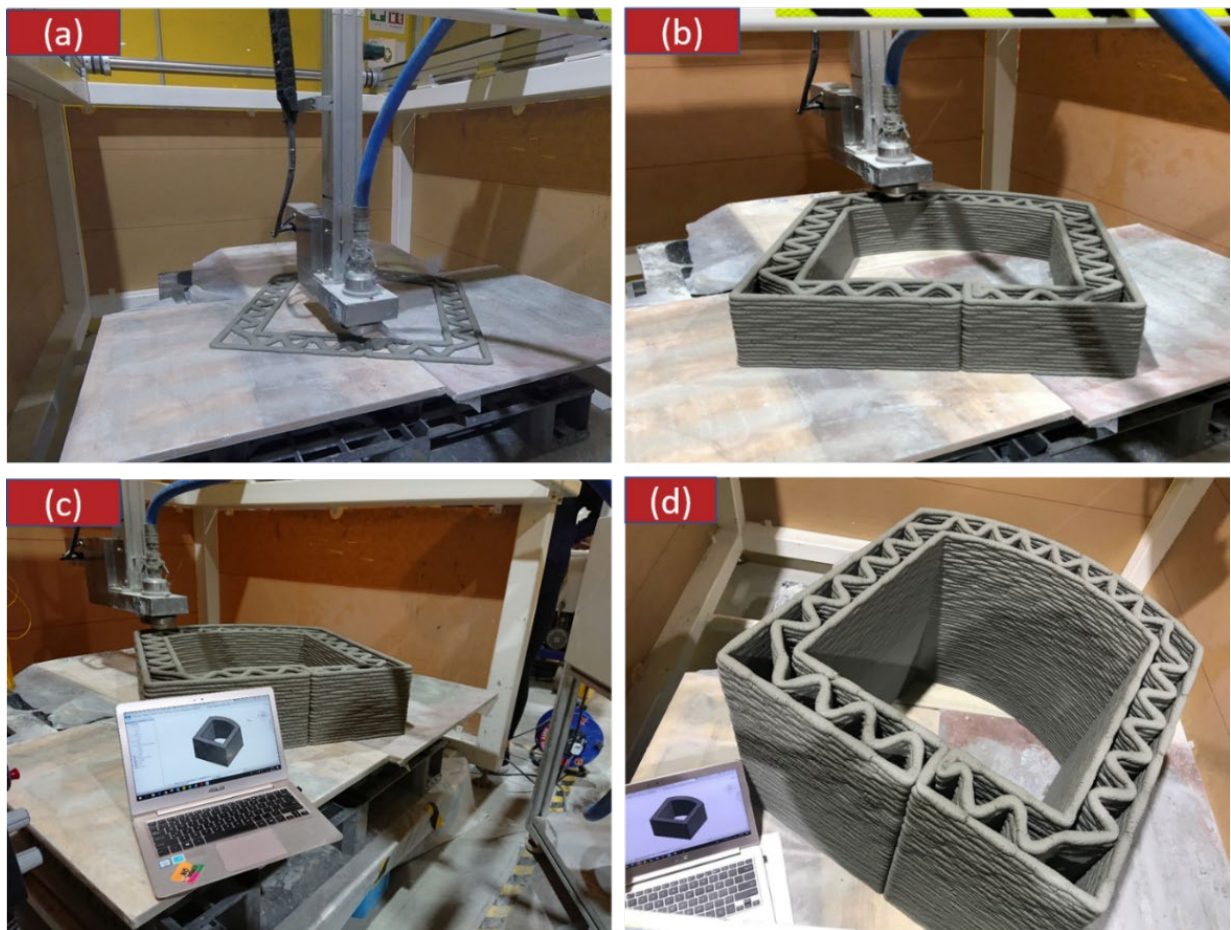


Fig. 19 Printing validation: (a) Printed structure after the 1st layer; (b) Printed structure after 17 layers; (c) Top view of the product being printed; (d) Final printed product (printing video can be found in supplemental material Video S1).

390

## 391 **Discussion and Future Work**

### 392 **Implications of Integrating BIM and 3DCP in The Construction Sector**

393 The 3D model used for 3DCP up to date is typically designed by 3D modeling software such as SolidWorks and  
394 Inventor. After the model is created, it needs to be exported as an STL file, sliced to generate the printing path, and  
395 converted to machine code for 3DCP. As a result, many efforts and time are involved in the data conversion process,  
396 and the quality and accuracy of the final data for practical printing may be affected (Wu et al. 2016a).

397

398 When the BIM platform is used for 3DCP, the workflow is still similar. The 3D model was created by BIM software  
399 like Revit, converted into an STL file, and then sliced by a 3D printing slicer (e.g., Cura, Slic3r). However, during the  
400 process, the BIM model might lose crucial information like material and structure type. Besides, the geometry  
401 information obtained by the conventional method may also be lost. On the other hand, for the proposed new approach,  
402 all the model processing is conducted within the BIM platform and, thus, all the material information and the geometry  
403 accuracy of the BIM model can be well reserved. Such a difference is especially apparent in the curvy structure. As  
404 shown in Fig. 20, the proposed approach can achieve a smoother and more accurate curve surface (Fig. 20 b) compared  
405 with that produced by the conventional method (Fig. 20 a), where the curvy structure consists of many segments. As  
406 a consequence, the final printed geometry accuracy will be impacted. Additionally, compared with the proposed new  
407 approach, the traditional method requires more time and unnecessary data transformation efforts. Therefore, it is  
408 imperative to integrate 3DCP with further developed construction targeted software (e.g., BIM software with a novel  
409 script in this work) to simplify the digital construction workflow and data transformation process.

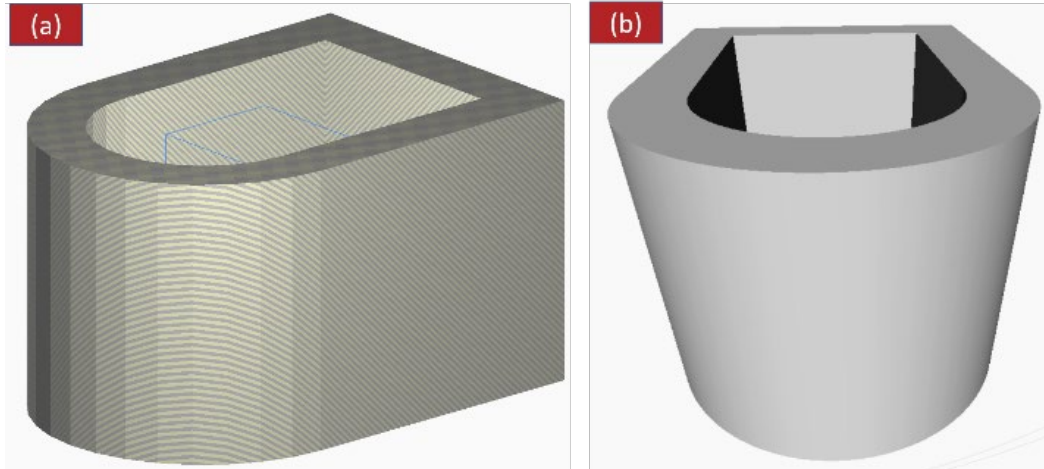


Fig. 20 Comparison between mesh models produced by: (a) the existing method and (b) the proposed method

Another limitation of the traditional method is the longer printing time due to the discontinuous printing path, which indicates that there are nozzle placement adjustments in the printing process. To quantify the printing time difference, various printing paths are generated by a widely used open-source slicer Slic3r and the proposed approach, respectively, as shown in Fig. 21. Assuming the gantry movement speed is the same (3000 mm/min) for all the printing paths, Fig. 21 (a) and (b) take 151 min and 148 min in the simulation, respectively. However, Fig. 21 (c) only needs 130 min for printing, which is approximately 12% less than that of traditional approaches. Since all the printing paths were generated with 20% infill, the extrusion time of printing paths (a) and (b) is the same as the printing path (c). Therefore, the time difference is mainly caused by the printing path discontinuity and nozzle placement adjustment.

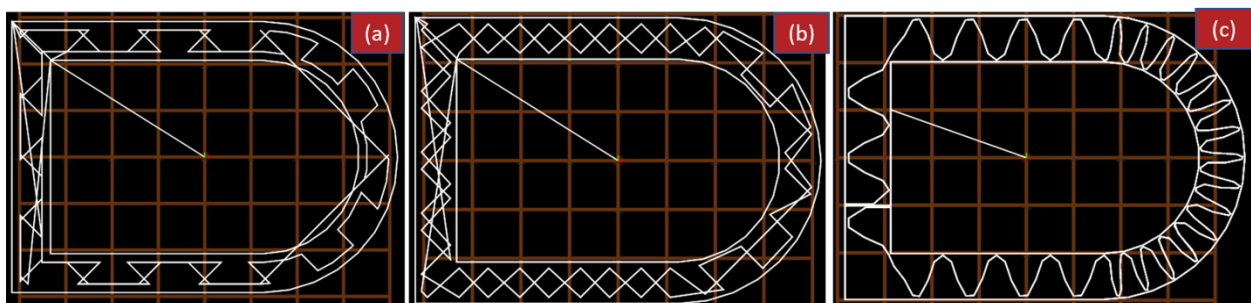


Fig. 21 Printing path with 20% infill produced by different methods with (a) 151 min printing time, created by Slic3r 1.30 from exported STL file; (b) 148 min printing time, created by Slic3r 1.29 from exported STL file; (c) 130 min printing time, created by the proposed approach with continuous printing path directly from BIM model

This work addresses the abovementioned issues and bridges the gap between BIM and 3DCP. A practical and straightforward method was proposed to integrate the workflow from BIM to 3DCP. In the proposed approach, a BIM authoring software integrated script package is developed to filter and slice a digital model, produce the continuous printing path, generate infills, create machine code, and send the machine code to a destination device. Afterward, the physical object can be printed by a 3D concrete printer. To demonstrate this novel fabrication process approach, the proposed script package was developed using Dynamo and integrated into BIM software Autodesk Revit; a digital model was designed in Autodesk Revit and printed by a 3D concrete printer.

In summary, the developed approach facilitates the implementation of BIM in 3DCP. The BIM file can be directly used for 3DCP instead of designing the printing model in other software. Considering the dimension and complexity of a construction project, substantial efforts and work hours can be saved from this integration. Additionally, the proposed method ensures better data quality for printing compared with the traditional approach since the process of converting the 3D model is more straightforward. Furthermore, it can enhance the coordination quality of designers and engineers in the construction sector.

#### **Future Work**

Preliminary work was conducted in this paper to integrate BIM with 3DCP for improving the productivity of digital fabrication in the construction sector. It was demonstrated to be practical and efficient, and a highly integrated system could be further developed to consolidate design, optimization, and fabrication to advance the AEC industry (Wu et al. 2016b).

To empower the integration further with material and structural optimization, a unified digital process is needed, as shown in Fig. 22. Close coordination among BIM modeling, 3DCP, and material and structural optimization is necessary to achieve the ultimate target, i.e., fabrication of a functional structure. BIM can be used to provide an integrated 3D information model to simulate building design as well as potential and alternative designs. During this process, material and structural optimization can be conducted by importing and verifying the data from BIM and optimization software (such as Abaqus), also considering the manufacturing constraints from 3D concrete printers. After the design is optimized, the physical objects will be fabricated through 3DCP, in which the processes are fully



controlled by BIM software. Furthermore, the designer can conduct further analysis of the printability and  
assemblability of the buildings through collaboration with manufacturing engineers; consequently, potential design  
improvements can be made. In summary, aided by structural optimization techniques and 3DCP, digital data managed  
through BIM can be potentially fully utilized for building planning, optimization, production, and assembly.

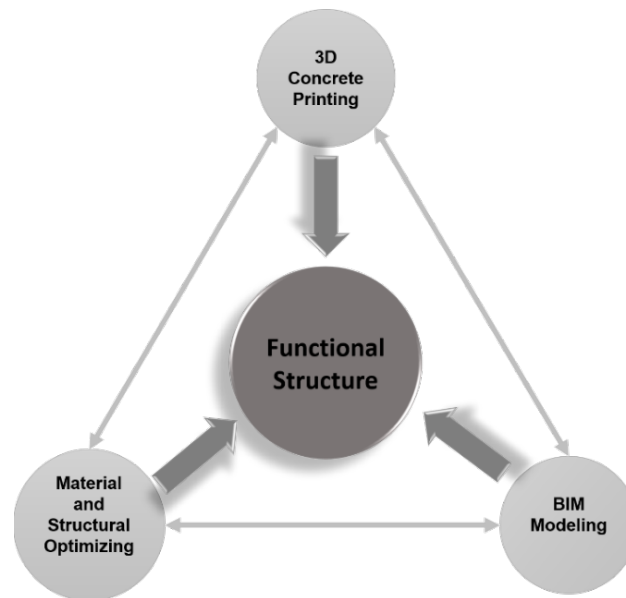


Fig. 22 A unified digital process combining design, optimization, and fabrication with the BIM platform and 3DCP

## Conclusions

BIM is a widely adopted industry platform for digital designing, management, and information sharing platform in the construction sector and has great potential to be integrated with 3D concrete printing for facilitating digital construction. This work proposes a novel fabrication process flow from BIM to 3D concrete printing (3DCP) by developing a script as a plug-in of Revit, which can simplify printing path generation and consequently reduce data loss and time consumption. To the author's knowledge, this is the first work in literature that proposes such a methodology to integrate BIM with 3DCP to promote digital construction development. As a result, the workflow from BIM software to 3DCP can be simplified, data interoperability and data loss during this process can be reduced, and 3DCP technology can be better integrated into the BIM platform.

The steps of the proposed background script package to automate filtering, slicing, infilling, and code generation are illustrated in detail. To demonstrate the feasibility and effectiveness of this novel approach, the proposed script



package was developed using Dynamo and integrated into BIM software Autodesk Revit; a digital model was designed in Autodesk Revit and printed by a 3D concrete printer.

This work is a preliminary study to bridge the gap between BIM data and 3DCP. Compared with the traditional method, there are many benefits of the proposed approach. Firstly, since all the operations and user interfaces are integrated within a single platform, the tedious task of transferring and processing data between different software in the traditional approach can be avoided. Secondly, this integration can also drastically reduce the errors due to software interoperability, transfer data losses, and file handling issues. These improvements have the potential to greatly shorten the time between design and construction, which would significantly improve productivity in the construction sector.

Because the script package is implemented in BIM software, various data like material type, resource planning, and stock availability can also be obtained in the fabrication process to create a genuinely autonomous and automated 3DCP process. In the future, 3DCP integrated with BIM and structural optimization software can potentially fully utilized for building planning, optimization, production, and assembly.

#### **Data Available Statement**

Some or all data, models, or codes that support the findings of this study are available from the corresponding author upon reasonable request, including the BIM model.

#### **Acknowledgments**

This research is supported by the National Research Foundation, Prime Minister's Office, Singapore under its Medium-Sized Centre funding scheme, Sembcorp Design & Construction Pte Ltd, and Sembcorp Architects & Engineers Pte Ltd.

#### **Disclaimer**

The authors declare no conflict of interest.

## Supplemental Materials

Figs. S1 – S6 and Video. S.1 are available online in the ASCE Library (ascelibrary.org).

## References

- Abdel-Wahab, Mohamed S., Andrew R. J. Dainty, Stephen G. Ison, Patrick Bowen, and Guy Hazlehurst. 2008. "Trends of Skills and Productivity in the UK Construction Industry." *Eng. Constr. Archit. Manag.* 15(4):372–382. doi: 10.1108/09699980810886865.
- Agarwal, Rajat, S. Chandrasekaran, and M. Sridhar. 2016. "Imagining Construction's Digital Future." Accessed August 5, 2019. <https://www.mckinsey.com/industries/capital-projects-and-infrastructure/our-insights/imagining-constructions-digital-future>.
- Arayici, Yusuf, P. Coates, Lauri Koskela, Mike Kagioglou, Colin Usher, and KJSS O'Reilly. 2011. "BIM Adoption and Implementation for Architectural Practices." *Struct. Surv.* 29(1):7–25. doi: 10.1108/02630801111118377.
- Bos, Freek, Rob Wolfs, Zeeshan Ahmed, Theo Salet, Rob Ahmed, Zeeshan, Theo Salet, Rob Wolfs, Zeeshan Ahmed, Theo Salet, Rob Ahmed, Zeeshan, Theo Salet, Rob Ahmed, Zeeshan Ahmed, and Theo Salet. 2016. "Additive Manufacturing of Concrete in Construction: Potentials and Challenges of 3D Concrete Printing." *Virtual Phys. Prototyp.* 11(3):209–225. doi: 10.1080/17452759.2016.1209867.
- Buswell, R., W. R. Silva, Jones. S.Z., and J. Dirrenberger. 2018. "3D Printing Using Concrete Extrusion: A Roadmap for Research." *Cem. Concr. Res.* 112:37–49. doi: 10.1016/j.cemconres.2018.05.006.
- Chang, Yi-Feng, and Shen-Guan Shih. 2013. "BIM-Based Computer-Aided Architectural Design." *Comput. Aided. Des. Appl.* 10(1):97–109. doi: 10.3722/cadaps.2013.97-109.
- Diggs-McGee, Brandy N., Eric L. Kreiger, Megan A. Kreiger, and Michael P. Case. 2019. "Print Time vs. Elapsed Time: A Temporal Analysis of a Continuous Printing Operation for Additive Constructed Concrete." *Addit. Manuf.* 28:205–214. doi: 10.1016/j.addma.2019.04.008.
- Ding, Lieyun, Ran Wei, and Haichao Che. 2014. "Development of a BIM-Based Automated Construction System." *Procedia Eng.* 85:123–131. doi: <https://doi.org/10.1016/j.proeng.2014.10.536>.
- Eastman, Chuck, Paul Teicholz, Rafael Sacks, and Kathleen Liston. 2011. *BIM Handbook: A Guide to Building Information Modeling for Owners, Managers, Designers, Engineers and Contractors*. 2nd ed. United States of America: John Wiley & Sons.

529 Elmulalim, Abbas, and Jonathan Gilder. 2014. "BIM: Innovation in Design Management, Influence and Challenges of  
530 Implementation." *Archit. Eng. Des. Manag.* 10(3–4):183–199. doi: 10.1080/17452007.2013.821399.

531 Fernandez-Vicente, Miguel, Wilson Calle, Santiago Ferrandiz, and Andres Conejero. 2016. "Effect of Infill  
532 Parameters on Tensile Mechanical Behavior in Desktop 3D Printing." *3D Print. Addit. Manuf.* 3(3):183–192.  
533 doi: 10.1089/3dp.2015.0036.

534 Gosselin, C., R. Duballet, Ph Roux, N. Gaudillière, J. Dirrenberger, and Ph Morel. 2016. "Large-Scale 3D Printing of  
535 Ultra-High Performance Concrete - a New Processing Route for Architects and Builders." *Mater. Des.* 100:102–  
536 109. doi: 10.1016/j.matdes.2016.03.097.

537 Herczeg, Márton, David McKinnon, Leonidas Milios, Ioannis Bakas, Erik Klaassens, Katarina Svatikova, and Oscar  
538 Widerberg. 2014. "Resource Efficiency in the Building Sector." *Copenhagen Resour. Inst.* Accessed  
539 November 13 2020. [https://ec.europa.eu/environment/eussd/pdf/Resource efficiency in the building sector.pdf](https://ec.europa.eu/environment/eussd/pdf/Resource%20efficiency%20in%20the%20building%20sector.pdf).

540 Jiang, Jingchao, Guobiao Hu, Xiao Li, Xun Xu, Pai Zheng, and Jonathan Stringer. 2019. "Analysis and Prediction of  
541 Printable Bridge Length in Fused Deposition Modelling Based on Back Propagation Neural Network." *Virtual  
542 Phys. Prototyp.* 14(3):253–266. doi: 10.1080/17452759.2019.1576010.

543 Khoshnevis, Behrokh. 2004. "Automated Construction by Contour Crafting - Related Robotics and Information  
544 Technologies." *Autom. Constr.* 13(1):5–19. doi: 10.1016/j.autcon.2003.08.012.

545 Le, T., S. Austin, S. Lim, R. Buswell, A. Gibb, and Tony Thorpe. 2012. "Mix Design and Fresh Properties for High-  
546 Performance Printing Concrete." *Mater. Struct.* 45(8):1221–1232. doi: 10.1617/s11527-012-9828-z.

547 Li, Mingyang, Lie Tang, Robert G. Landers, and Ming C. Leu. 2013. "Extrusion Process Modeling for Aqueous-  
548 Based Ceramic Pastes—Part 2: Experimental Verification." *J. Manuf. Sci. Eng.* 135(5):051009.

549 Lim, E. C., and J. Alum. 1995. "Construction Productivity: Issues Encountered by Contractors in Singapore." *Int. J.  
550 Proj. Manag.* 13(1):51–58. doi: 10.1016/0263-7863(95)95704-H.

551 Lim, Jian Hui, Yiwei Weng, and Quang-cuong Pham. 2020. "3D Printing of Curved Concrete Surfaces Using  
552 Adaptable Membrane Formwork." *Constr. Build. Mater.* 232:117075. doi: 10.1016/j.conbuildmat.2019.117075.

553 Lo, Tommy Y., Ivan W. Fung, and Karen C. Tung. 2006. "Construction Delays in Hong Kong Civil Engineering  
554 Projects." *J. Constr. Eng. Manag.* 132(6):636–649. doi: 10.1061/(ASCE)0733-9364(2006)132:6(636).

555 Lu, Bing, Yiwei Weng, Mingyang Li, Ye Qian, Kah Fai Leong, Ming Jen Tan, and Shunzhi Qian. 2019. "A  
556 Systematical Review of 3D Printable Cementitious Materials." *Constr. Build. Mater.* 207:477–490. doi:

10.1016/j.conbuildmat.2019.02.144.

Nasir, Hassan, Hani Ahmed, Carl Haas, and Paul M. Goodrum. 2014. "An Analysis of Construction Productivity Differences between Canada and the United States." *Constr. Manag. Econ.* 32(6):595–607. doi: 10.1080/01446193.2013.848995.

Rashid, Ans Al, Shoukat Alim Khan, Sami G. Al-ghamdi, and Muammer Koç. 2020. "Additive Manufacturing : Technology , Applications , Markets , and Opportunities for the Built Environment." *Autom. Constr.* 118:103268. doi: 10.1016/j.autcon.2020.103268.

Salet, Theo A. M., Zeeshan Y. Ahmed, Freek P. Bos, and Hans L. M. Laagland. 2018. "Design of a 3D Printed Concrete Bridge by Testing Design of a 3D Printed Concrete Bridge by Testing." *Virtual Phys. Prototyp.* 13(2):222–236. doi: 10.1080/17452759.2018.1476064.

De Schutter, Geert, Karel Lesage, Viktor Mechtcherine, Venkatesh Naidu Nerella, Guillaume Habert, and Isolda Agusti-Juan. 2018. "Vision of 3D Printing with Concrete — Technical, Economic and Environmental Potentials." *Cem. Concr. Res.* 112:25–36. doi: 10.1016/j.cemconres.2018.06.001.

Tibaut, Andrej, Danijel Rebolj, and Matjaž Nekrep Perc. 2016. "Interoperability Requirements for Automated Manufacturing Systems in Construction." *J. Intell. Manuf.* 27(1):251–262. doi: 10.1007/s10845-013-0862-7.

Wang, Qiancheng, Hsi-Hsien Wei, and Qian Xu. 2018. "A Solid Oxide Fuel Cell (SOFC)-Based Biogas-from-Waste Generation System for Residential Buildings in China: A Feasibility Study." 10(7):2395. doi: 10.3390/su10072395.

Weng, Yiwei, Mingyang Li, Shaoqin Ruan, Teck Neng Wong, Ming Jen Tan, Kah Leong, Ow Yeong, and Shunzhi Qian. 2020. "Comparative Economic, Environmental and Productivity Assessment of a Concrete Bathroom Unit Fabricated through 3D Printing and a Precast Approach." *J. Clean. Prod.* 261:121245. doi: 10.1016/j.jclepro.2020.121245.

Weng, Yiwei, Bing Lu, Mingyang Li, Zhixin Liu, Ming Jen Tan, and Shunzhi Qian. 2018. "Empirical Models to Predict Rheological Properties of Fiber Reinforced Cementitious Composites for 3D Printing." *Constr. Build. Mater.* 189:676–685. doi: 10.1016/j.conbuildmat.2018.09.039.

Weng, Yiwei, Shaoqin Ruan, Mingyang Li, Liwu Mo, Cise Unluer, Ming Jen Tan, and Shunzhi Qian. 2019. "Feasibility Study on Sustainable Magnesium Potassium Phosphate Cement Paste for 3D Printing." *Constr. Build. Mater.* 221:595–603. doi: 10.1016/j.conbuildmat.2019.05.053.

585 Wu, Peng, Jun Wang, and Xiangyu Wang. 2016a. "A Critical Review of the Use of 3-D Printing in the Construction  
586 Industry Material Finished." *Autom. Constr.* 68:21–31. doi: 10.1016/j.autcon.2016.04.005.

587 Wu, Peng, Jun Wang, and Xiangyu Wang. 2016b. "A Critical Review of the Use of 3-D Printing in the Construction  
588 Industry Material Finished." *Autom. Constr.* 68:21–31. doi: 10.1016/j.autcon.2016.04.005.

589 Xia, Ming, Behzad Nematollahi, and Jay Sanjayan. 2019. "Printability, Accuracy and Strength of Geopolymer Made  
590 Using Powder-Based 3D Printing for Construction Applications." *Autom. Constr.* 101:179–189. doi:  
591 10.1016/j.autcon.2019.01.013.

592

## 594

	OPC	Sand		SF	Water	SP	Accelerator
		F <sub>1</sub>	F <sub>2</sub>				
Weight/g	48,800	8,050	8,050	4,879	13,600	75	150

595